SPE 59309

Pore-Scale Modeling of Three-Phase Flow and the Effects of Wettability

Mun-Hong Hui, Stanford University and Martin J. Blunt, Imperial College

This paper was prepared for presentation at the 2000 SPE/DOE Improved Oil Recovery Symposium held in Tulsa, Oklahoma, 3–5 April 2000.

Abstract

We analyze fluid configurations in a single pore for three-phase flow in mixed-wet systems. After primary drainage solid surfaces in contact with oil may alter their wettability. We consider waterflooding followed by gas injection for any possible combination of oil/water, gas/water and gas/oil contact angles. We compute capillary pressures for the different displacement processes, find the range of capillary pressures for which the various fluid configurations are stable, and obtain expressions for the fluid saturations and conductances.

We compute three-phase relative permeabilites for a bundle of tubes of different size with constant triangular cross-sections. We model gas injection starting from different initial oil saturations, S_{oi}. We show that the oil remains connected in wetting layers down to low oil saturation with a characteristic layer drainage regime. The only exceptions are non-spreading oils in water-wet media and large gas/oil contact angles. The relative permeability of the phase of intermediate wettability depends on both its own saturation and S_{oi}, while the other relative permeabilities are functions of their own saturation only. In water-wet media, oil is the intermediate-wet phase. In weakly oil-wet media, water is intermediate-wet. In most strongly oil-wet media, gas is intermediate-wet. This contradicts the assumptions made in many empirical models that gas is always the most non-wetting phase and that its relative permeability depends only on the gas saturation. For media that contain regions of different wettabilitites, all three relative permeabilities may depend on both their own saturation and S_{oi}.

This work indicates appropriate functional dependencies for three-phase relative permeabilities, as well as being a necessary first step towards the development of a realistic three-dimensional, three-phase predictive pore-scale model that accounts for the effects of wettability.

Introduction

Three-phase flow occurs in oil reservoirs during solution gas drive, gas cap expansion, gas injection and thermal flooding. Prediction of the flow behavior in these cases requires estimates of three-phase relative permeabilities and capillary pressures. Direct measurements of three-phase properties are often difficult and time consuming to obtain. Instead, extrapolations from two-phase measurements are typically used. For example, in Prudhoe Bay where significant oil recovery comes from three-phase gravity drainage and gas injection, there have been few core experiments where all three phases were flowing simultaneously. To predict the behavior in reservoir modeling studies, extensive two-phase data have been used as a basis of a detailed empirical three-phase model.[1,2]

Pore-scale modeling offers an appealing alternative to empirical models for predicting three-phase relative permeability. Micromodel experiments and theoretical analysis have elucidated the microscopic three-phase displacement mechanisms in water-wet and oil-wet media.[3-8] These studies have been the basis of pore network models that predict macroscopic parameters from the pore structure and the displacement physics.[9-13] However, this work assumed that the medium was strongly water-wet. The behavior for the full range of possible oil/water, gas/oil and gas/water contact angles has not been studied. Furthermore, pores do not necessarily have a uniform wettability, but may contain regions with different contact angles.[14,15]

Two-phase network models to study the effects of wettability have been developed by several authors. Any oil/water contact angle could be assigned to each pore in the network.[16-19] Kovscek et al.[20] developed a physically-based model for wettability alteration at the pore scale. A primary drainage displacement was first simulated, assuming that the medium is initially fully water-saturated and water-wet. Where oil directly contacted the solid surface, the surface became strongly oil-wet. Regions of the pore where wetting layers or thick wetting films were present, as well as pores full of water, remained water-wet. Capillary pressures where computed for a bundle of star-shaped pores. Blunt extended this model to allow the regions of the pore space contacted by

oil to assume any oil/water contact angle.[21,22] He computed relative permeabilites and capillary pressures for a three-dimensional network containing pores with a square cross-section. Øren et al.[23] used a similar model of the displacement physics and wettability changes to simulate two-phase flow in a network with a random topology that was reconstructed from thin section analysis. The predicted relative permeability of a mixed-wet reservoir rock agreed with experimental measurements. Man and Jing studied the effects of wettability on electrical resistivity.[24] Overall, the effects of wettability on relative permeability and oil recovery for two-phase flow are now reasonably well understood.[19,21]

This paper is one step in the three-phase extension of the two-phase work described above. The model of Kovscek et al.[20] and Blunt[21] will be used to find the pore-scale configurations of oil, water and gas during waterflooding and gas injection, for the full range of possible oil/water, gas/oil and gas/water contact angles. As in Kovscek et al.,[20] the general trends in behavior with wettability will be studied using a bundle-of-tubes model.

The purpose of this work is twofold. First, the description of fluid configurations, displacement capillary pressures and conductances for three-phase mixed-wet pores is a necessary first step in the development of a predictive three-phase network model that will combine these displacement mechanisms with a realistic description of the pore space in a three-dimensional network. Second, the analysis of relative permeabilities, albeit from an idealized model, illustrates some general features that will be present in more sophisticated treatments. As such they serve as a guide for the development of empirical three-phase relative permeability models and as a way of interpreting experimental results.

First, the different possible pore-scale configurations will be described and the capillary pressures for displacement from one configuration to another will be given. Then the fluid saturations and conductances will be found. Finally, these results will be used in a bundle-of-capillary-tubes model to predict trends in three-phase relative permeability as the wettability of the system is modified.

Primary Drainage and Wettability Change

We will consider pores with a uniform polygonal cross-section. Each corner of the polygon has a half-angle α. Later we will consider one specific case: pores whose cross-sections are equilateral triangles where $\alpha = \pi/6$. While the assumption of angular pores is simplistic, it does allow the corner of the pores to be filled with wetting fluid, even if the centers are filled with another phase. As we will show, flow through these wetting layers has a significant impact on relative permeability.

Initially all the pores are full of water and the system is strongly water-wet. This represents the native state of the reservoir before primary oil migration. First primary drainage is simulated. The oil/water capillary pressure P_{cow} is increased. Oil enters a pore at:[25]

$$P_{cow} = \frac{\sigma_{ow} C}{R} \quad \text{.....(1)}$$

where σ_{ow} is the oil/water interfacial tension, R is the inscribed radius of curvature of the pore and:

$$C = \cos\theta_0 + \sqrt{\frac{\tan\alpha}{2}\left(\sin 2\theta_0 - 2\theta_0 - 2\alpha + \pi\right)} \quad \text{.....(2)}$$

θ_0 is the oil/water contact angle during primary drainage, which is assumed to be zero. Primary drainage continues until some maximum capillary pressure $P_{cow}^{\max}$ is reached.

Surfaces of the pore in direct contact with oil can alter their wettability through the deposition of surface active components in the crude, called asphaltenes.[14,20,26] We assume that the wettability changes for all these surfaces. However, small pores that are water-filled remain water-wet, as do the corners of the pore that still contain water. The oil/water contact angle for primary drainage on the surfaces of altered wettability is θ_1, which allows for some rearrangement of the fluid in the pore space. Since further drainage moves the oil over previously water-coated surfaces, θ_1 is close to θ_0. We assume $\theta_1 + \alpha < \pi/2$, and thus water is always present in the corners. The fluid configuration at the end of primary drainage is shown in **Fig. 1** for a pore that has been invaded by oil. The distance b of water-wet surface is:

$$b = \frac{\sigma_{ow}}{P_{cow}^{\max}}\left(\cot\alpha\cos\theta_1 - \sin\theta_1\right) \quad \text{.....(3)}$$

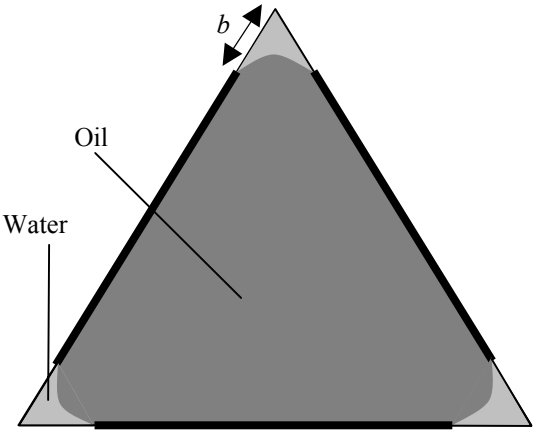

Fig.1. Oil and water in a triangular pore after primary drainage. The areas directly contacted by oil (shown by the bold line) have an altered wettability, while the corners that are water-filled remain water-wet. *b* is the length of the water-wet surface.

During waterflooding and gas injection, we will allow any value for the oil/water, gas/water and gas/oil contact angles at the surfaces of altered wettability. While this is a simple model of wettability alteration, it captures one of the principal mechanisms for wettability alteration in reservoir settings,[14,26]

and for two-phase flow has been shown to lead to macroscopic consequences that cover the full range of experimentally observed behavior.[19-21] The essential features of the model are: (1) different wettabilities may be present in a single pore, as shown by electron microscopy;[15] (2) any combination of contact angles can be considered; and (3) the mechanism of wettability alteration is the contact of crude oil with the solid surface.[14,26]

The different possible arrangements of the three phases in a single pore are illustrated in **Fig. 2**. Configuration A represents a water-filled pore that was not invaded during primary drainage and so remains water-wet. We will assume that these pores are never invaded during gas injection, although this could be considered by setting $\theta_{gw} = 0$ in the equations that follow. Below we will describe how the other configurations arise during water and gas injection.

Waterflooding

The advancing oil/water contact angle for waterflooding, θ_{ow} may be larger than θ_l. As the oil/water capillary pressure decreases the oil/water/solid contact is pinned with a hinging contact angle θ_h that increases from θ_l to θ_{ow}. When $\theta_h = \theta_{ow}$ the oil/water/solid contact can move and displacement may occur. There are three possible displacement mechanisms for pore filling: spontaneous snap-off, piston-like advance and forced snap-off. These mechanisms have already been described for mixed-wet pores by Blunt.[21] Here we will use more accurate expressions for the capillary pressures for piston-like advance based on Øren et al.[23]

Spontaneous Snap-off. Spontaneous snap-off only occurs when $\theta_{ow} + \alpha < \pi/2$, when the water layer in the corner can swell at a positive oil/water capillary pressure — configuration B in Fig.2. When the water layers lose contact with the solid surface, the pore spontaneously fills with water to give configuration D at an oil/water capillary pressure:

$$P_{cow} = \frac{\sigma_{ow}\left(\cos\theta_{ow} - \sin\theta_{ow}\tan\alpha\right)}{R} \quad \ldots\ldots\ldots\ldots\ldots\ldots\ldots\ldots(4)$$

Forced Snap-off. Forced snap-off occurs for $P_{cow} < 0$, when $\theta_{ow} + \alpha \geq \pi/2$. Here the oil/water/solid contact point remains pinned – configuration C in Fig. 2, and the hinging contact angle varies continually with capillary pressure until the oil/water contact angle reaches θ_{ow}, when the oil/water interface bulges out into the center of the pore. When the hinging contact angle is θ_{ow}, the oil/water/solid contact begins to move and the pore spontaneously fills with water to reach configuration D. The capillary pressure for this displacement is:

$$P_{cow} = \frac{\sigma_{ow}\left(\cot\alpha\cos\theta_{ow} - \sin\theta_{ow}\right)}{b} \qquad \pi - \alpha \geq \theta_{ow} \geq \pi/2 - \alpha \quad \ldots(5)$$

$$= -\frac{\sigma_{ow}}{b\sin\alpha} \qquad \theta_{ow} > \pi - \alpha$$

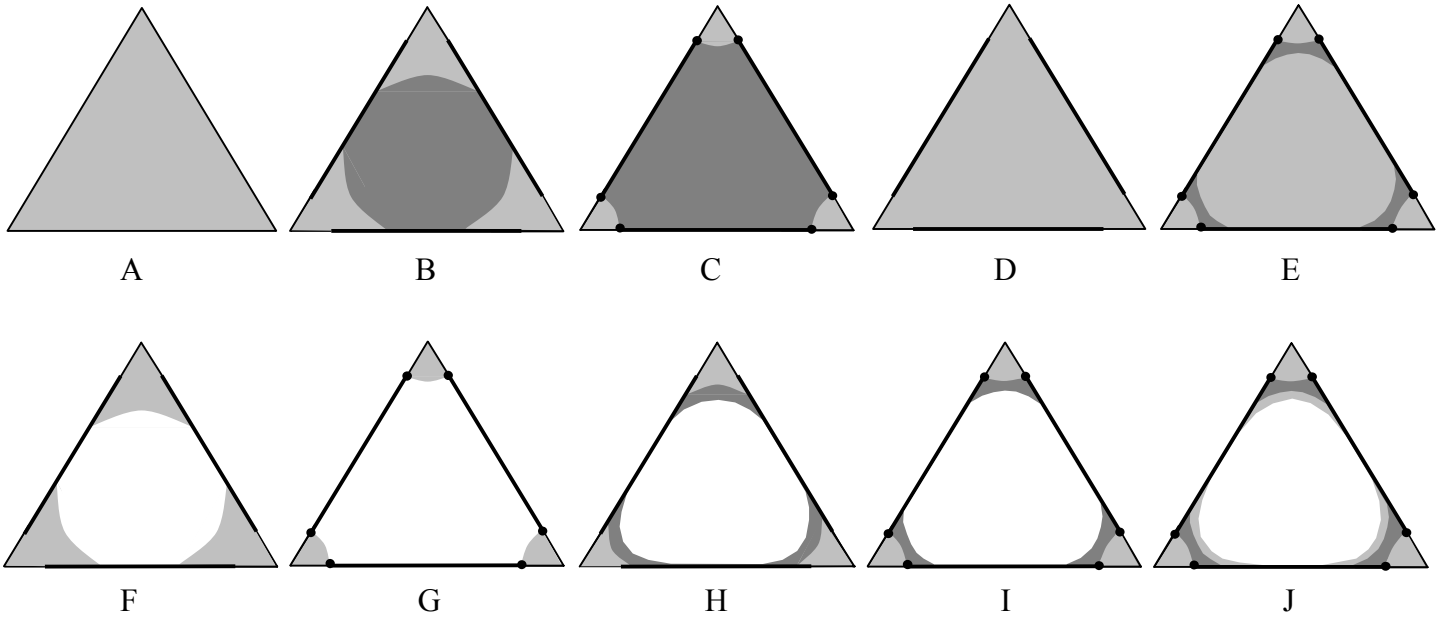

Fig. 2. The different pore-scale configurations for waterflooding and gas injection in mixed-wet pores. A bold line indicates regions of the pore space with altered wettability. The solid circles indicate points where the fluid/surface contact is pinned and the contact angle continually varies with capillary pressure. Light gray indicates water, dark gray oil and white is gas.

Piston-like Advance. The capillary pressures for piston-like advance are found from the Mayer-Stowe-Princen (MSP) theory.[27-30] There are three different expressions depending on the contact angle. For contact angles less than a critical value θ_{crit}, water spontaneously imbibes into the pore with a positive capillary pressure. After invasion the pore is completely filled with water – the displacement goes from configuration B or C to D in Fig. 2. θ_{crit} may be greater than $\pi/2$, since water advances into pores containing both water in the corners, where the effective contact angle is zero, as well as bare surfaces along the sides, with a contact angle θ_{ow} The critical angle for spontaneous imbibition θ_{crit} is given by:

$$\cos\theta_{crit} = -\frac{\sin(\alpha+\theta_1)\sin\alpha}{\frac{RP_{cow}^{\max}}{\sigma_{ow}}\cos\alpha - \cos(\alpha+\theta_1)} \quad \text{.....(6)}$$

To obtain the capillary pressure for the displacement, the following equations are solved:

$$P_{cow} = \frac{\sigma_{ow}\Omega_{eff}}{A_{eff}} = \frac{\sigma_{ow}}{r} \quad \text{.....(7)}$$

r is the effective mean radius of curvature and:

$$A_{eff} = \frac{R^2}{2\tan\alpha} - \frac{rb\sin(\alpha+\beta)}{2} + \frac{r^2\beta}{2} \quad \text{.....(8)}$$

$$\Omega_{eff} = \left(\frac{R}{\tan\alpha} - b\right)\cos\theta_{ow} + r\beta \quad \text{.....(9)}$$

$$r\sin\beta = b\sin\alpha \quad \text{.....(10)}$$

To solve these equations, P_{cow} is first computed assuming that $r = R$. The angle β is found from Eq. (10). Then Eqs. (8) and (9) are used to find A_{eff} and Ω_{eff} and a new value of r is obtained from Eq. (7). A converged value of r and P_{cow} to three significant figures is normally found in just 3 iterations.

For $\theta_{ow} > \theta_{crit}$ water injection is forced, with a negative capillary pressure. For $\pi/2 + \alpha \geq \theta_{ow} > \theta_{crit}$, the displacement is from configuration C to D in Fig. 2, at a capillary pressure:

$$P_{cow} = \frac{2\sigma_{ow}\cos\theta_{ow}}{R} \quad \text{.....(11)}$$

Oil Layer Formation and Stability. After piston-like advance with $\theta_{ow} > \pi/2 + \alpha$ there is water in the center of the pore, and water in the corners, with a layer of oil sandwiched in between – configuration E in Fig. 2. The capillary pressure for displacement in this case is similar to Eqs. (1)-(2) for primary drainage:

$$P_{cow} = \frac{\sigma_{ow}C}{R} \quad \text{.....(12)}$$

$$C = \cos\theta_{ow} - \sqrt{\frac{\tan\alpha}{2}\left(-\sin 2\theta_{ow} + 2\theta_{ow} - 2\alpha - \pi\right)} \quad \text{....(13)}$$

The oil layers are stable until the two arcs touch each other, when it is assumed that the layers spontaneously collapse. We go from configuration E to D. This occurs at a capillary pressure:

$$P_{cow} = \frac{\sigma_{ow}\left[\cos\alpha\sin\alpha\left(2\sin\alpha + \cos\theta_{ow}\right) + \sin^2\alpha \times \sqrt{4\cos^2\alpha - 3 - \cos^2\theta_{ow} - 4\sin\alpha\cos\theta_{ow}}\right]}{b\left(3\sin^2\alpha + 4\sin\alpha\cos\theta_{ow} + \cos^2\theta_{ow}\right)} \quad \text{.....(14)}$$

Gas Injection

We assign gas/water and gas/oil contact angles, θ_{gw} and θ_{go} respectively, for gas injection. The displacement is always piston-like advance, since gas is not initially present in wetting layers. The gas/water and gas/oil capillary pressures increase. We assume that $P_{cgw} = P_{cow} + P_{cgo}$. We also assume that the gas pressure is never high enough to displace water from water-filled pores that have never had oil in them — configuration A in Fig. 2.

Gas Invasion into Water. If $\theta_{gw} < \pi/2 - \alpha$ gas may fill the center of a pore while water occupies the corners, without a pinned gas/water/solid contact. Gas invasion is a displacement from configuration D in Fig. 2 to F, or from configuration E to J. The capillary pressure is similar to that for primary drainage:

$$P_{cgw} = \frac{\sigma_{gw}}{R}\left(\cos\theta_{gw} + \sqrt{\frac{\tan\alpha}{2}\left(\sin 2\theta_{gw} - 2\theta_{gw} - 2\alpha + \pi\right)}\right) \quad \text{.....(15)}$$

For $\theta_{gw} \geq \pi/2 - \alpha$, the gas/water/solid contact is pinned. Gas invasion is a displacement from configuration D in Fig. 2 to G, or from E to I. The capillary pressure is:

$$P_{cgw} = \frac{2\sigma_{gw}\cos\theta_{gw}}{R} \quad \text{.....(16)}$$

Gas Invasion into Oil. The displacement capillary pressures are similar to those for gas injection into water. If $\theta_{go} < \pi/2 - \alpha$ gas invasion is a displacement from configuration B to H, or from C to I. There is a free gas/oil/solid contact, resulting in an oil layer sandwiched between water in the corners and gas in the center of the pore. The displacement capillary pressure is:

$$P_{cgo} = \frac{\sigma_{go}}{R}\left(\cos\theta_{go} + \sqrt{\frac{\tan\alpha}{2}\left(\sin 2\theta_{go} - 2\theta_{go} - 2\alpha + \pi\right)}\right) \quad \text{.....(17)}$$

For $\theta_{go} \geq \pi/2 - \alpha$ oil layers cannot be formed. The displacement goes from configuration B to F, or C to G, at a capillary pressure:

$$P_{cgo} = \frac{2\sigma_{go}\cos\theta_{go}}{R} \quad \text{.....(18)}$$

Layer Formation and Stability. For gas injection there are three fluid configurations with layers of either oil or water – H, I and J in Fig. 2. For oil layers to be present sandwiched between water and gas – configurations H or I, we must have:

$$\theta_{go} + \alpha < \frac{\pi}{2} \quad \text{.....(19)}$$

Configuration H in Fig. 2 is where a layer of oil is sandwiched between water and gas at a positive oil/water capillary pressure. Such a layer will only exist if:

$$\theta_{ow} + \alpha < \frac{\pi}{2} \quad \text{.....(20)}$$

In H the oil/water contact has moved during water injection, so that it is no longer pinned. This is only true if the oil/water capillary pressure exceeds:

$$P_{cow} = \frac{\sigma_{ow}\left(\cot\alpha\cos\theta_{ow} - \sin\theta_{ow}\right)}{b} \quad \text{.....(21)}$$

Notice that this capillary pressure is the same as for forced snap-off, Eq. (5). The difference here is that $P_{cow} > 0$ and thus the oil/water/solid contact is stable.

Oil layer stability depends on the ratio of oil/water to gas/oil interfacial curvatures:

$$R_o = \frac{r_{ow}}{r_{go}} = \frac{\sigma_{ow}P_{cgo}}{\sigma_{go}P_{cow}} \quad \text{.....(22)}$$

Oil layers are stable in configuration H for $R_o \leq R_{co}$, where:

$$R_{co} = \frac{\cos(\theta_{go} + \alpha)}{\cos(\theta_{ow} + \alpha)} \quad \text{.....(23)}$$

if $\theta_{go} \geq \theta_{ow}$. The oil layers collapse when the oil/water/solid and gas/oil/solid contact points meet and we go from configuration H to F. For $\theta_{go} < \theta_{ow}$ the oil/water and gas/oil interfaces first meet at their centers. Again we have a transition from H to F at a critical curvature ratio:

$$R_{co} = \frac{\cos\theta_{go} - \sin\alpha}{\cos\theta_{ow} - \sin\alpha} \quad \text{.....(24)}$$

If the oil/water/solid interface is pinned – configuration I in Fig. 2 – the oil/water capillary pressure is less than the critical value given in Eq. (21). To determine oil layer stability we first find the hinging contact angle from:

$$\theta_h = \cos^{-1}\left(\frac{P_{cow}b\sin\alpha}{\sigma_{ow}}\right) - \alpha \quad \text{.....(25)}$$

If $\theta_{go} \geq \theta_h$ then we use Eq. (23) with θ_h substituted for θ_{ow} to determine whether or not oil layers are stable. If $\theta_h > \theta_{go}$ then we use Eq. (24) with θ_h substituted for θ_{ow}.

The final case is configuration J in Fig. 2, where there are layers of both water and oil. Oil layer collapse is a transition from configuration J to F. The criterion for oil layer stability is given by Eq. (14). The water layers are sandwiched between oil and gas. The water layer stability is determined in the same way as for oil layers. Water layer collapse is a transition from J to I. We only see water layers if the following two conditions are met:

$$\theta_{gw} + \alpha < \frac{\pi}{2} \quad \text{.....(26)}$$

$$\theta_{ow} > \frac{\pi}{2} + \alpha \quad \text{.....(27)}$$

Then defining:

$$R_w = \frac{r_{ow}}{r_{gw}} = \frac{\sigma_{ow}P_{cgw}}{\sigma_{gw}P_{cow}} \quad \text{.....(28)}$$

Water layers are stable for $R_w \leq R_{cw}$, where:

$$R_{cw} = \frac{\cos(\theta_{gw} + \alpha)}{\cos(\theta_{ow} + \alpha)} \quad \text{.....(29)}$$

for $\theta_{gw} \geq \pi - \theta_{ow}$. For $\theta_{gw} < \pi - \theta_{ow}$:

$$R_{cw} = \frac{\cos\theta_{gw} - \sin\alpha}{\cos\theta_{ow} + \sin\alpha} \quad \text{.....(30)}$$

Fluid Saturation and Conductance

We will compute the three-phase relative permeabilities as a function of saturation for a bundle of parallel pores. The saturation of each phase is the sum of the cross-sectional areas of each phase in each pore, divided by the total areas of all the pores. The relative permeability is the sum of the conductances in each pore, divided by the sum of conductances if only a single phase fills all the pores.

The total area of a pore of inscribed radius R is:

$$A_t = n_c R^2 \cot\alpha \quad \text{.....(31)}$$

where n_c is the number of corners in each pore.

Each pore has a fixed length L and has a fixed pressure difference ΔP imposed across each phase. The conductance g is defined by:

$$Q = \frac{g}{\mu}\frac{\Delta P}{L} \quad \text{.....(32)}$$

where Q is the volume of fluid flowing per unit time and μ is the viscosity.

For a pore totally full of a single fluid, we use the following approximation for g based on Poiseuille's law for flow in a circular cylinder:[31]

$$g = \frac{\pi\left(\sqrt{A_t/\pi} + R\right)^4}{128} \quad \text{.....(33)}$$

For a phase that occupies the center of the pore space, we use the same expression, but with A_t substituted by the area of the phase.

The area occupied by fluid occupying the corners of a pore, with an interfacial radius of curvature r is:

$$A_c = n_c r^2\left[\cos\theta\left(\cot\alpha\cos\theta - \sin\theta\right) + \theta + \alpha - \pi/2\right] \text{....(34)}$$

where θ is the contact angle. Eq. (34) is valid for all values of θ.

If a non-wetting phase occupies the center of the pore and a wetting phase occupies the corners with $\theta + \alpha < \pi/2$, the wetting phase conductance can be found from an approximate expression due to Zhou et al.[32]

$$g = \frac{A_c^2(1-\sin\alpha)^2(\phi_2\cos\theta - \phi_1)\phi_3^2}{12n_c\sin^2\alpha(1-\phi_3)^2(\phi_2 + f\phi_1)^2} \quad \text{.....(35)}$$

where:

$$\phi_1 = \frac{\pi}{2} - \alpha - \theta \quad \text{.....(36)}$$

$$\phi_2 = \cot\alpha\cos\theta - \sin\theta \quad \text{.....(37)}$$

$$\phi_3 = \left(\frac{\pi}{2} - \alpha\right)\tan\alpha \quad \text{.....(38)}$$

f is used to indicate the boundary condition at the fluid/fluid interface. f = 1 represents a no-flow boundary, while f = 0 is a free boundary. We will assume f = 1 for all oil/water interfaces and f = 0 for all gas/water and gas/oil interfaces. This is in agreement with results of two and three-phase flow experiments in single capillary tubes.[33]

Although Eq. (35) is an algebraically complex expression, it can easily be used in network modeling studies to compute the conductance of wetting fluid. It gives predictions close to results obtained from direct computations of the Navier-Stokes equation in a corner.[34]

For $\theta + \alpha > \pi/2$ the fluid/fluid interface bulges out into the center of the pore and Eq. (35) is no longer valid. To find an approximate expression for the conductance in this case, we write Eq. (35) in terms of the corner area and α when θ = 0:

$$g = \frac{A_c^2\tan\alpha(1-\sin\alpha)^2\phi_3^2}{12n_c\sin^2\alpha(1-\phi_3)(1+f\phi_3)^2} \quad \text{.....(39)}$$

We use this expression when $\theta + \alpha > \pi/2$ using Eq. (34) with the appropriate **non-zero** value of θ to find A_c.

Zhou et al.[32] also derived an expression for the conductance of an oil layer sandwiched between water and gas, as in configuration H of Fig. 2. Here it is assumed that $\theta_{go} = \theta < \pi/2 - \alpha$ and $\theta_{ow} = 0$. The conductance is:

$$g = \frac{A_c^2(1-\sin\alpha)^2\left(\phi_2\cos\theta - \phi_1 - \cot\alpha(1-\phi_3)R_o^2\right)^3\phi_3^2}{\left\{\begin{array}{l}12n_c\sin^2\alpha(1-\phi_3)^2(\phi_2\cos\theta - \phi_1)^2\times \\ (\phi_2 + f_1\phi_1 - \cot\alpha(1-f_2\phi_3)R_o)^2\end{array}\right\}} \cdots$$

$$\text{.....(40)}$$

where f_1 is the boundary condition at the gas/oil interface and f_2 is the boundary condition at the oil/water interface. R_o is given by Eq. (22). The corner area is the area of both the oil layer **and** the water in the corners. The corner area is found from Eq. (34) with $\theta = \theta_{go}$ and $r = r_{go} = \sigma_{go}/P_{cgo}$.

For cases with a non-zero oil/water contact angle, or interfaces that bulge into the centers of the pore space, we use a modified version of Eq. (40) to find the oil layer conductance. First we re-write Eq. (40) assuming zero contact angles:

$$g = \frac{A_o^3(1-\sin\alpha)^2\tan\alpha\phi_3^2}{12n_cA_c\sin^2\alpha(1-\phi_3)\left(1 + f_1\phi_3 - (1-f_2\phi_3)\sqrt{\frac{A_w}{A_c}}\right)^2} \cdots$$

$$\text{.....(41)}$$

A_w is the area of water in the corners computed from Eq. (34) with $\theta = \theta_{ow}$ and $r = r_{ow} = \sigma_{ow}/P_{cow}$. A_o is the area of oil in the corners. $A_o = A_c - A_w$, where A_c is given by Eq. (34) with $\theta = \theta_{go}$ and $r = r_{go} = \sigma_{go}/P_{cgo}$. Eq. (41) is then used to find the oil layer conductance with non-zero values of the contact angle. With a suitable substitution of subscripts, the same approach can be used for oil layers sandwiched between water, or for water layers, as described below.

These equations will form the basis of the analysis to follow. The conductance equations are approximate – for first-principles predictive modeling it may be appropriate to use expressions that are based on direct solution of the Navier Stokes equation for each pore.[23,34]

Primary Drainage. For a pore completely full of water, Eq. (31) is used to find the water area in each pore and Eq. (33) is used to compute the water conductance. For a pore with oil in the center and water in the corners, the water area is found from Eq. (34) with $\theta = \theta_1$ and $r = r_{ow} = \sigma_{ow}/P_{cow}$, and the water conductance from Eq. (35) with $\theta = \theta_1$ and f = 1. The oil area A_o is $A_t - A_c$. The oil conductance is found from Eq. (33) but with A_o substituted for A_t.

Waterflooding. Again if oil or water occupy the center of a pore Eq. (33) is used to find the conductance but with A_t substituted by the oil or water area in the center of the pore. The area of fluid in the pore center is the total area of the pore minus the area of water in the corners and oil layers, if present.

To find the water areas in the corners, the hinging contact angle is first calculated from Eq. (25). If $\theta_h < \theta_{ow}$, then the oil/water/solid interface is pinned, and Eq. (34) is used to find the water area with $\theta = \theta_h$ and $r = r_{ow} = \sigma_{ow}/P_{cow}$. If $\theta_h \geq \theta_{ow}$ then Eq. (34) is used with $\theta = \theta_{ow}$. For $\theta + \alpha < \pi/2$, Eq. (35) is used to find the water conductance with $f = 1$. If $\theta + \alpha > \pi/2$, then Eq. (39) is used, again with $f = 1$.

If oil layers are present – configuration E in Fig. 2 – then we use Eq. (41) to find the oil layer conductance. Here $f_1 = f_2 = 1$. A_c is the area of the oil layer plus the area of water in the corners. A_c is found from Eq. (34) with $\theta = \pi - \theta_{ow}$ and $r = r_{ow} = \sigma_{ow}/P_{cow}$. A_w is the water area in the corners. Eq. (25) is used to find the hinging contact angle of the pinned contact and then A_w is found from Eq. (34) with $\theta = \theta_h$ and $r = r_{ow} = \sigma_{ow}/P_{cow}$. The oil layer area $A_o = A_c - A_w$.

With oil layers present, the water conductance and area have two components – from water in the corners and water in the pore center. The total areas and the conductances are the sum of these two contributions.

Gas Injection. Gas always occupies the center of the pore space. Thus Eq. (33) is used for the gas phase conductance with the area of gas A_g substituted for A_t. A_g is the total area of the pore minus the area of water in the corners and any water and oil layers.

For configuration F in Fig. 2, where $\theta_{gw} + \alpha < \pi/2$, the water area in the corners is found from Eq. (34) with $\theta = \theta_{gw}$ and $r = r_{gw} = \sigma_{gw}/P_{cgw}$. The water conductance is found from Eq. (35) with $f = 0$ and $\theta = \theta_{gw}$.

For configuration G in Fig. 2, the gas/water/solid interface is pinned. First the hinging contact angle is computed using Eq. (25) with P_{cgw}/σ_{gw} substituted for P_{cow}/σ_{ow}. Eq. (34) is used to find the water area with $\theta = \theta_h$ and $r = r_{gw} = \sigma_{gw}/P_{cgw}$. For $\theta_h + \alpha < \pi/2$, Eq. (35) is used to find the water conductance with $f = 0$. If $\theta_h + \alpha \geq \pi/2$, then Eq. (39) is used, again with $f = 0$.

For configuration H in Fig. 2 we have $\theta_{ow} + \alpha < \pi/2$ and $\theta_{go} + \alpha < \pi/2$. Eq. (34) is used to find the water area A_w with $\theta = \theta_{ow}$ and $r = r_{ow} = \sigma_{ow}/P_{cow}$. Eq. (35) with $f = 1$ is used to find the water conductance with $A_c = A_w$. The area of water and oil in the corners A_c is found from Eq. (34) $\theta = \theta_{go}$ and $r = r_{go} = \sigma_{go}/P_{cgo}$. The oil area $A_o = A_c - A_w$. Then Eq. (41) with $f_1 = 0$ and $f_2 = 1$ is used to find the oil layer conductance.

In configuration I in Fig. 2, the oil/water/solid contact is pinned and $\theta_{go} + \alpha < \pi/2$. The hinging oil/water contact angle is computed using Eq. (25). Eq. (34) is used to calculate A_w with $\theta = \theta_h$ and $r = r_{ow} = \sigma_{ow}/P_{cow}$. Eq. (39) with $f = 1$ is used for the water conductance with $A_c = A_w$. A_c is found from Eq. (34) with $\theta = \theta_{go}$ and $r = r_{go} = \sigma_{go}/P_{cgo}$. The oil area $A_o = A_c - A_w$. The oil layer conductance is then found from Eq. (41) with $f_1 = 0$ and $f_2 = 1$.

In configuration J in Fig. 2 we have water in both the corners and in a layer, as well as an oil layer. The oil/water/solid contact is pinned and $\theta_{gw} + \alpha < \pi/2$. The hinging contact angle is computed using Eq. (25). Eq. (34) is used to calculate A_{wc} the area of water in the corners with $\theta = \theta_h$ and $r = r_{ow} = \sigma_{ow}/P_{cow}$. Eq. (40) with $A_c = A_{wc}$ and $f = 1$ is used for the water conductance. The oil layer conductance is computed as for configuration E. The area of oil plus water $A_o + A_{wc}$ is found from Eq. (34) with $\theta = \pi - \theta_{ow}$ and $r = r_{ow} = \sigma_{ow}/P_{cow}$. Eq. (41) is used to find the oil layer conductance with $A_c = A_o + A_{wc}$, $A_w = A_{wc}$ and $f_1 = f_2 = 1$. If the area of the water layer is A_{wl}, the area of all the water and the oil layer $A_o + A_{wc} + A_{wl}$ is found from Eq. (34) with $\theta = \theta_{gw}$ and $r = r_{gw} = \sigma_{gw}/P_{cgw}$. Eq. (41) with $f_1 = 0$ and $f_2 = 1$ is used to find the water layer conductance by substituting A_o in Eq. (41) with A_{wl}, A_w with $A_o + A_{wc}$ and $A_c = A_o + A_{wc} + A_{wl}$. The total water conductance is the sum of the conductances of water in the corners and the water layer. The total water area $A_w = A_{wc} + A_{wl}$.

Network Model

We consider displacement in a parallel bundle of horizontally aligned pores. Each pore has the same length and has an equilateral triangular cross-section ($\alpha = \pi/6$), but the pores have different inscribed radii. We use a truncated Weibull distribution with 50 pores similar to Fenwick and Blunt.[11] The inscribed pore radii are found from:

$$R = \left(R_{\max} - R_{\min}\right)\left(-\delta \ln\left[x\left(1 - e^{-1/\delta}\right) + e^{-1/\delta}\right]\right)^{1/\gamma} + R_{\min} \quad \ldots\ldots (42)$$

where x is a random number between 0 and 1. The parameters used in the distribution are shown in **Table 1**.

We simulate primary drainage, waterflooding and gas injection and compute relative permeabilities and capillary pressures as a function of saturation. We assume that the capillary pressures alone control the displacement sequence, which is applicable for low flow rates. We fill one pore at a time. During primary drainage P_{cow} increases and at each step oil occupies pores with the lowest value of P_{cow} for displacement. Primary drainage ends at $P_{cow}^{\max}$ when the water occupies only a small number of the smallest pores, and the corners of the larger oil-filled pores. The water saturation at the end of primary drainage is 2% for all the cases presented. During waterflooding P_{cow} decreases, and at each step water invades the pore with the highest value of P_{cow} for displacement. Since we consider only a bundle of tubes, all of which are accessible for displacement, we need only consider piston-like advance. Snap-off will only occur in multidimensional networks when piston-like advance is topologically impossible.[21] Waterflooding ceases at an oil

saturation S_{oi}. During gas flooding the gas pressure increases. We fill pores in sequence with the pore that will be invaded at the lowest gas pressure filled first. This may be gas displacing oil, controlled by $P_{cgo} = P_g - P_o = P_g - P_w - P_{cow}$, or gas displacing water controlled by $P_{cgw} = P_g - P_w$. We assume that during gas injection P_{cow} remains constant at its value at the end of waterflooding. The simulations continue until there is no further displacement of oil by gas.

We compute the relative permeability and saturation of each phase after each pore is filled. We use the layer stability equations to check whether or not layers of oil and/or water are present.

We study two fluid systems: one based on air/water/hexane and the other based on air/water/dodecane. The interfacial tensions used are shown in **Table 2**. Simulations are performed for different combinations of contact angles and S_{oi}. The different properties used are listed in **Table 3**.

Parameter	Meaning	Value
R_{min}	Minimum pore radius	1 μm
R_{max}	Maximum pore radius	18.5 μm
δ	Exponent	0.8
γ	Exponent	1.6

Table 1. Parameters used for the distribution of inscribed pore radius, *R*, Eq. (42).

System	σ_{gw} (mN/m)	σ_{go} (mN/m)	σ_{ow} (mN/m)
Hexane	67	19	48
Dodecane	71	23	51

Table 2. Interfacial tensions for the two fluid systems studied. The data comes from Firincioglu et al.[33]

Possible Values of the Contact Angles. There is one constraint on the interfacial tensions and contact angles. Consider the oil/water/solid contact on a flat surface illustrated in **Fig. 3**. A horizontal force balance gives:

$$\sigma_{os} = \sigma_{ws} + \sigma_{ow}\cos\theta_{ow} \quad \text{.....(43)}$$

where σ_{ws} is the water/solid interfacial tension and σ_{os} is the oil/surface interfacial tension. We can consider equivalent situations with water/gas/solid and oil/gas/solid contacts to obtain:

$$\sigma_{gs} = \sigma_{ws} + \sigma_{gw}\cos\theta_{gw} \quad \text{..... (44)}$$

$$\sigma_{gs} = \sigma_{os} + \sigma_{go}\cos\theta_{go} \quad \text{.....(45)}$$

where σ_{gs} is the gas/solid interfacial tension. Adding Eqs. (43) and (45) and comparing with Eq. (44) leads to:[35]

$$\sigma_{gw}\cos\theta_{gw} = \sigma_{go}\cos\theta_{go} + \sigma_{ow}\cos\theta_{ow} \quad \text{.....(46)}$$

Eq. (46) assumes that all three phases are stationary and in thermodynamic equilibrium and that the interfacial tensions include the effects of any wetting and spreading films that may be present. It is not known how applicable this expression is when the contacts are moving over a rough and chemically heterogeneous surface. However, we will use it as a constraint on our values of contact angles.

Case	System	θ_{ow} (degrees)	θ_{go} (degrees)	θ_{gw} (degrees)	S_{oi}
1	Hexane	20	0	17	0.90
2	Hexane	20	0	17	0.35
3	Dodecane	20	30	17	0.90
4	Hexane	70	0	58	0.90
5	Dodecane	70	30	58	0.90
6	Hexane	180	0	116	0.90
7	Hexane	180	0	116	0.35
8	Hexane	95	0	77	0.90
9	Hexane	95	0	77	0.35

Table 3. Contact angles and initial oil saturations at the beginning of gas injection for the different simulations run. In all cases $\theta_l = 20^o$.

Contact Angles for a Water-Wet Medium. If the system is strongly water-wet the solid surfaces are coated by a thick film of water making $\sigma_{gs} = \sigma_{gw}$ and $\sigma_{os} = \sigma_{ow}$, which leads to the following expression for θ_{go} from Eq. (45):[36]

$$\cos\theta_{go} = \frac{\sigma_{gw} - \sigma_{ow}}{\sigma_{go}} = 1 + \frac{C_{so}}{\sigma_{go}} \quad \text{.....(47)}$$

where C_{so} is the oil spreading coefficient, defined by:

$$C_{so} = \sigma_{gw} - \sigma_{ow} - \sigma_{go} \quad \text{.....(48)}$$

In thermodynamic equilibrium, where the gas/water interface may include a molecular spreading film of oil, $C_{so} \le 0$.[37] Several authors have discussed the effect of C_{so} on oil recovery, which is due to its influence on oil layer stability, Eqs. (23) and (24).[10-12,35,38-41]

We study a spreading oil, hexane ($C_{so} = \theta_{go} = 0$), and a non-spreading oil, dodecane ($C_{so} < 0$ and $\theta_{go} = 30^o$). For simplicity we will use Eq. (47) to find θ_{go} even when the system is not water-wet.

Contact Angles for an Oil-Wet Medium. Consider an oil-wet system where the solid surfaces are coated by a thick oil film. Then in Eq. (44) $\sigma_{gs} = \sigma_{go}$ and $\sigma_{ws} = \sigma_{ow}$, which leads to:

$$\cos\theta_{gw} = \frac{\sigma_{go} - \sigma_{ow}}{\sigma_{gw}} \quad \text{.....(49)}$$

For most fluid systems – even at reservoir conditions – $\sigma_{ow} > \sigma_{go}$ meaning that $\theta_{gw} > 90^o$. Gas is wetting to water in strongly oil-wet media. Measurements of contact angles on oil-wet

surfaces that have found θ_{gw} in the range 100° – 120°, consistent with predictions based on Eq. (49).[33,40]

If we obey Eq. (46), gas is only non-wetting to water for water-wet and weakly oil-wet media. For $\theta_{gw} < 90°$ the largest possible value of θ_{ow} is around 110°. This means that we cannot have configuration J with a water layer in Fig. 2 for our hexane system in a triangular pore, since this requires $\theta_{gw} < 60°$ and $\theta_{ow} > 120°$ (Eqs. (26) and (27)).

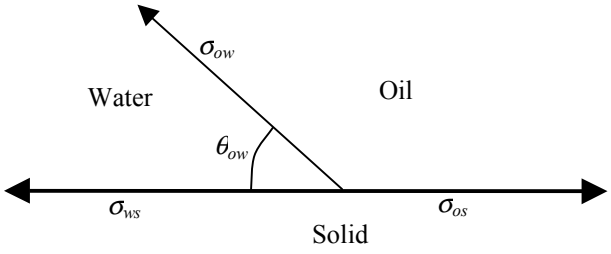

Fig. 3. Three-phase oil/water/solid contact. Considering the horizontal balance of forces for this and the oil/gas/solid and water/gas/solid contacts leads to a relation between the interfacial tensions and contact angles, Eq. (46).

Wettability Types. There are three different generic wettability types. The first is a water-wet system, where gas is non-wetting to both water and oil. Here water is the most wetting phase, gas is non-wetting and oil is intermediate-wet. The second type is a strongly oil-wet medium, where gas is wetting to water, but non-wetting to oil. Here oil is the most wetting phase, water is non-wetting and gas is intermediate-wet. The third case is a weakly oil-wet medium, where gas is non-wetting to both oil and water. Oil is the wetting phase, gas is non-wetting and water is intermediate-wet. On physical grounds we do not consider cases where gas is more wetting than oil. We will now explore the consequences of these different wettabilities on relative permeability.

To define our systems we use the interfacial tensions for either the hexane or dodecane system, we use Eq. (47) to determine θ_{go}, we specify different values of θ_{ow} and then use Eq. (46) to find θ_{gw}. The different values of contact angle are listed in Table 3.

Two-Phase Relative Permeability. Fig. 4 shows the oil and water relative permeabilities for water injection for case 1 (θ_{ow} = 20°) and case 6 (θ_{ow} = 180°). For case 1, the water preferentially invades the smallest pores first. In contrast, for case 6, the water preferentially invades the largest pores, resulting in a higher water relative permeability and a lower oil relative permeability. The primary drainage relative permeabilities for all cases are the same as for water injection for case 1.

A bundle of capillary tubes model does not show any hysteresis, unless a wettability change occurs during the displacement sequence. Furthermore, no trapping can be observed. Thus the two-phase behavior of this model is rather simple. However, the same pore level physics, used in a three-dimensional network, has revealed a complex structure of hysteresis and trends in residual oil saturation with contact angle.[21,22]

Oil Layer Drainage. Fig. 5 shows the oil relative permeability during gas injection for water-wet media – cases 1 and 3. The difference between these two cases is the spreading coefficient of the oil, which manifests itself in different values of the gas/oil contact angle (Table 3). Oil layers collapse at a higher gas/oil capillary pressure for hexane (R_{co} = 1.35 in Eq. (24)) than for dodecane (R_{co} = 0.78 in Eq. (23)). This means that for hexane oil layers remain until all the oil-filled pores have been invaded by gas and very low oil saturations – less than 1% – are reached, whereas for dodecane, the oil saturation is around 8% when the layers collapse. In a three-dimensional network, the oil phase is likely to become disconnected when the layers are no longer present, and oil is trapped.

Before the oil layers collapse, the dodecane relative permeability is slightly higher than for hexane. For the same number of pores filled with gas, the hexane relative permeability is higher than dodecane, because oil layers make a greater contribution to the overall conductance. However, there is also more oil in these layers. If we compare relative permeabilities at the same oil saturation, this second effect dominates – hexane occupies fewer pores than dodecane, with the extra saturation coming from layers. The extra conductance from these layers fails to compensate for the effect of having fewer oil-filled pores, making the hexane relative permeability slightly lower than for dodecane. This counter-intuitive effect where allowing layer flow decreases the oil relative permeability at moderate to low saturations is apparent in three-phase core data.[44]

At low oil saturation, for case 1, we see approximately $k_{ro} \sim S_o^2$. This quadratic form of the relative permeability is a consequence of the expression used for oil layer conductance, Eq. (41). Once gas has invaded most of the oil-filled pores, the oil saturation is approximately proportional to the oil area A_o. The oil layer conductance (Eq. (41)), and hence the relative permeability, is approximately, although not exactly, proportional to A_o^2, assuming that A_w is smaller or roughly the same size as A_o. The effect of spreading coefficient on oil recovery, as well as the quadratic behavior of the oil relative permeability has already received extensive theoretical discussion[7,10,32] and has been confirmed experimentally.[7,33,39,40]

Fig. 6 shows the oil relative permeability for intermediate-wet and oil-wet media – cases 4, 5 and 6. We see oil layer drainage to low saturation with an approximately quadratic form for the relative permeability for all these cases, including the dodecane system. The oil/water/solid contacts are pinned, meaning that the oil/water interface cannot move to meet the gas/oil interface, initiating layer collapse. Oil layer collapse

only occurs at a high gas/oil capillary pressure once gas has invaded all the oil-filled pores, and has pushed almost all the oil out of the corners.

The oil relative permeability is sensitive to both the gas/oil and oil/water contact angles. This is due to the equations used for oil layer conductance and area. As before, the dodecane system has a slightly higher relative permeability, for the same reason as in Fig. 5. The oil-wet hexane system has the lowest oil relative permeability. This is because the oil/water capillary pressure is negative, and the oil/water interface bulges out towards the gas/oil interface (configuration I of Fig. 2). This leads to a lower oil layer conductance compared with weakly water-wet systems, where the oil/water interface bulges towards the corner, since $P_{cow} > 0$. Notice the subtle competition between oil layer area and conductance – in some cases a large layer area tends to decrease relative permeability when comparing configurations with the same overall oil saturation, whereas in other cases, the greater conductance of these layers increases the relative permeability.

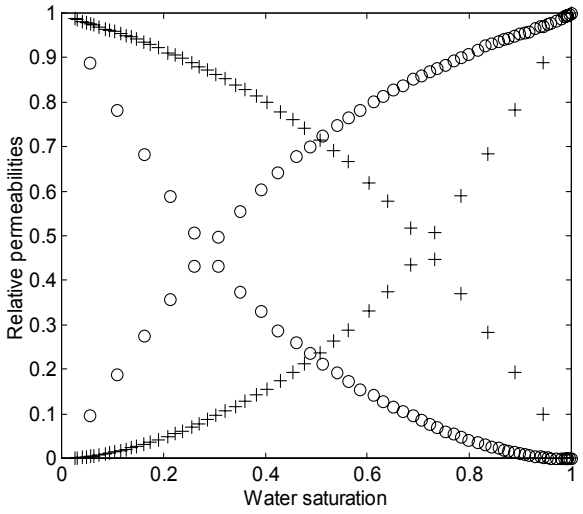

Fig. 4. Two-phase relative permeabilities for water injection. The crosses are for a water-wet system, case 1 (θ_{ow} = 20°) and the circles are for an oil-wet system, case 6 (θ_{ow} = 180°).

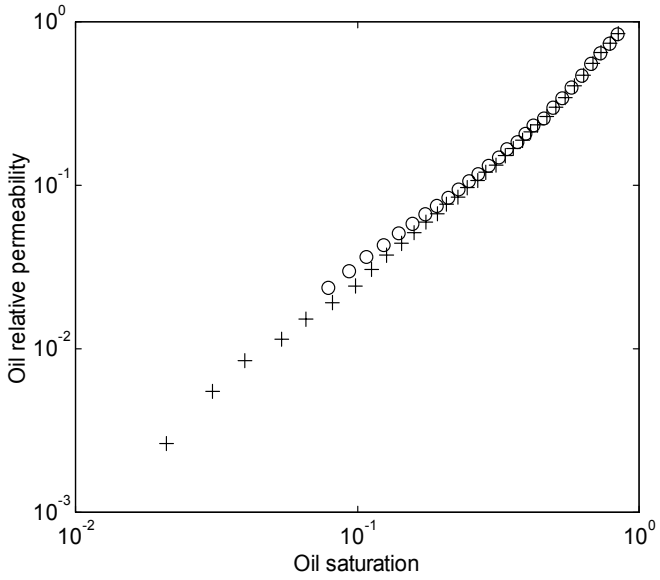

Fig. 5. Oil relative permeability during gas injection in water-wet media. The crosses are for a hexane system, case 1 (θ_{go} = 0) and the circles are for a dodecane system, case 3 (θ_{go} = 30°). The curve for case 3 is stopped at around S_o = 0.08, when oil layers collapse. For case 1, oil layers are present until a high gas/oil capillary pressure when the oil saturation is less than 1%.

The oil remains connected in layers during gas injection with a characteristic layer drainage regime. For three-dimensional systems, this will allow oil to drain to very low saturations, giving potentially high oil recoveries for gas injection. The two exceptions to this are non-spreading oils in water-wet media (case 3), or situations where oil layers can never form, which we haven't studied, where Eq. (19) is not obeyed — $\theta_{go} + \alpha > \pi/2$.

The full consequences of oil layer connectivity and stability can be only be explored using a three-dimensional network. The gas pressure at which layers collapse depends on the capillary pressure reached during primary drainage, through its effect on b, and the oil/water capillary pressure during waterflooding. Hence the oil relative permeability during gas injection may be sensitive to the whole previous displacement sequence.

Three-Phase Relative Permeabilities. While the relative permeability at low saturation may be dominated by layer drainage, the high saturation behavior is controlled by the size of pores occupied by each phase. In the results that follow we will see only three generic types of relative permeability. The first is for the wetting phase that occupies the smallest pores. The second is for the most non-wetting phase that occupies the largest pores. In both these cases the relative permeability is insensitive to S_{oi}. The relative permeability of the intermediate-wet phase lies between the wetting and non-wetting extremes and is function of both its own saturation and S_{oi}.

Oil Intermediate-Wet. Fig. 7 shows the water, oil and gas relative permeabilities for cases 1 and 2. Water is the wetting phase, gas is non-wetting and oil is intermediate-wet. The gas relative permeability is a function of the gas saturation only and does not depend on S_{oi}. For water, since gas preferentially invades oil before water, we see only isolated values of the relative permeability. However, the points lie on the two-phase curve for a water-wet system – Fig. 4. The water relative permeability depends only on the water saturation.

To understand the oil relative permeability, consider the schematic pore occupancies shown in **Fig. 8.** If S_{oi} is large, oil

occupies almost all the pores at the beginning of gas injection. Gas then invades the large oil-filled pores. Hence oil is left filling the smaller pores. In contrast, if S_{oi} is small, oil only occupies the larger pores initially. While gas will preferentially invade the largest of these, at the same oil saturation, oil will occupy larger pores than for a case with high S_{oi}, resulting in a higher oil relative permeability. The oil relative permeability for gas injection is thus a function of both S_o and S_{oi}, as shown in Fig. 7. For modeling gas injection processes, this means that k_{ro} is a function of two independent saturations, while k_{rg} and k_{rw} are functions of their own saturations only. This observation is already well known theoretically,[43-45] and has been confirmed experimentally.[45-50]

Gas Intermediate-Wet. Fig. 9 shows the three-phase relative permeabilities for cases 6 and 7, where the system is strongly oil-wet. Here oil is the most wetting phase, water is non-wetting and gas is the intermediate-wet phase. Using similar arguments as before, we see from Fig. 9 that the oil relative permeability is similar to the water relative permeability for a water-wet system and is independent of S_{oi}. This has been seen experimentally.[40] The water relative permeability is also independent of S_{oi} and is similar to the gas relative permeability in Fig. 7, although not identical, since water continues to reside in the corners of the pores. Since gas is intermediate-wet, it is now the gas relative permeability that depends on both S_g and S_{oi}. This is an important observation, since many empirical models of three-phase relative permeability assume that the gas relative permeability is a function of gas saturation only.[1,2,42,43]

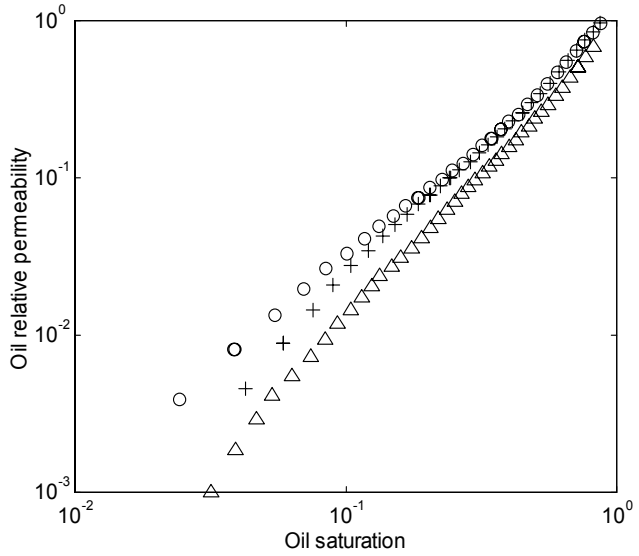

Fig. 6. Oil relative permeability during gas injection. The crosses are for a weakly water-wet hexane system, case 4 (θ_{go} = 0 and θ_{ow} = 70°), the circles are for a weakly water-wet dodecane system, case 5 (θ_{go} = 30° and θ_{ow} = 70°), and the triangles are for an oil-wet hexane system, case 6 (θ_{go} = 0 and θ_{ow} = 180°). All three cases show a layer drainage regime to low oil saturation.

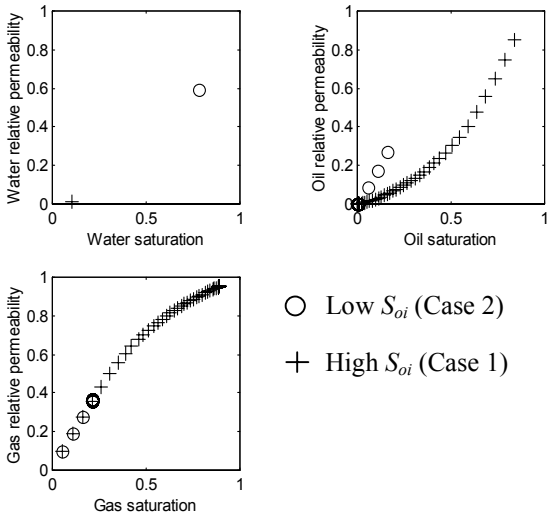

Fig. 7. Three-phase relative permeabilities for a water-wet system. Oil is the intermediate-wet phase. The gas and water relative permeabilities do not depend on S_{oi}, while the oil relative permeability does. This result can be explained by considering the sizes of the pores occupied by each phase — Fig. 8.

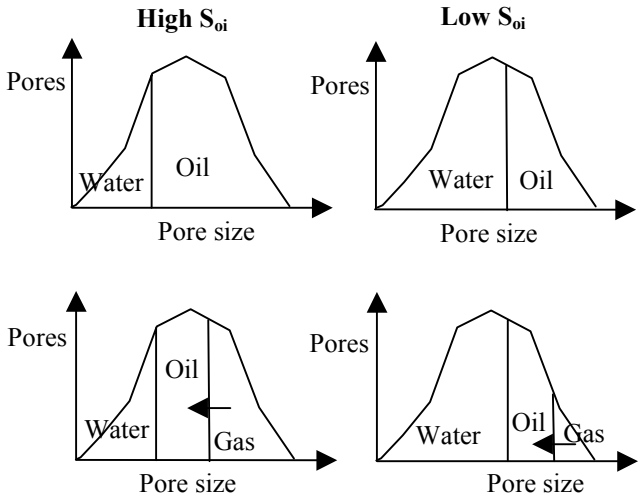

Fig. 8. Schematic pore occupancies for a water-wet system. For two-phase flow, water resides in the small pores and oil in the large pores. During gas injection, the gas displaces oil from the largest pores. As the diagram shows, for the same oil saturation, oil will be in larger pores for low S_{oi} than for high S_{oi}, resulting in a higher oil relative permeability.

At the beginning of gas injection we can compare the gas pressure necessary to enter a water-filled pore, as against an oil-filled pore. For gas to displace water we use Eq. (16):

$$P_g = P_w + P_{cgw} = P_w + \frac{2\sigma_{gw}\cos\theta_{gw}}{R_{gw}} \quad \text{.....(50)}$$

where R_{gw} is the inscribed radius of the pore to be filled by gas. For a gas/oil displacement:

$$P_g = P_w + P_{cow} + P_{cgo}$$
$$\approx P_w + \frac{2\sigma_{ow}\cos\theta_{ow}}{R_{ow}} + \frac{2\sigma_{go}\cos\theta_{go}}{R_{go}} \quad \ldots\ldots\ldots\ldots\ldots\ldots(51)$$

R_{ow} is the inscribed radius of the pore last filled by water and R_{go} is the inscribed radius of the pore to be filled by gas. We have used approximate forms for the oil/water and gas/oil capillary pressures. Since the medium is oil-wet, R_{ow} will represent the smallest water-filled pore. Gas is wetting to water and so will want to fill this smallest pore. Hence $R_{gw} = R_{ow}$. Gas is non-wetting to oil and so fills the largest oil-filled pores first. Hence $R_{go} \approx R_{ow}$. We now compare Eqs. (50) and (51) with Eq. (46), to see that the gas pressures to displace oil and water are about the same. This means that gas will displace both water and oil, starting with pores with a radius R_{ow}, which is set by the capillary pressure at the end of water injection. This is shown schematically in **Fig. 10.** If R_{ow} is large (large S_{oi}), then the gas relative permeability is higher than if R_{ow} is small (small S_{oi}), as seen in Fig. 9. Notice that for low S_{oi} the points tend to come in bunches in Fig. 9, with closely spaced points followed by larger gaps. A point is plotted each time a pore is filled. Gas is displacing both oil from small pores and water from large pores. The points close together represent the filling of the small pores, while the gaps represent filling large pores.

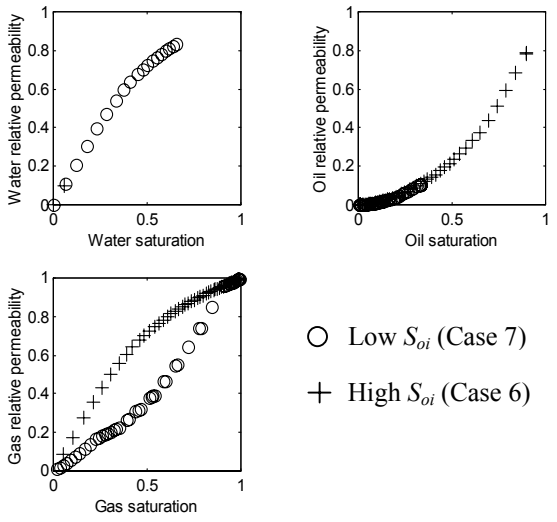

Fig. 9. Three-phase relative permeabilities for a strongly oil-wet system. Gas is the intermediate-wet phase. The oil and water relative permeabilities do not depend on S_{oi}, while the gas relative permeability does.

Water Intermediate-Wet. Fig. 11 shows the third generic combination of contact angles: an oil-wet system, where gas is non-wetting to both water and oil. Gas always fills the largest pores, while oil resides in the smallest pores. Water is intermediate-wet and its relative permeability is sensitive to S_{oi}, while the gas and oil relative permeabilities are functions of only their own saturations. The schematic pore occupancy is shown in **Fig. 12** which illustrates why the water relative permeability is higher for large S_{oi}, since at the same water saturation, the water is in larger pores.

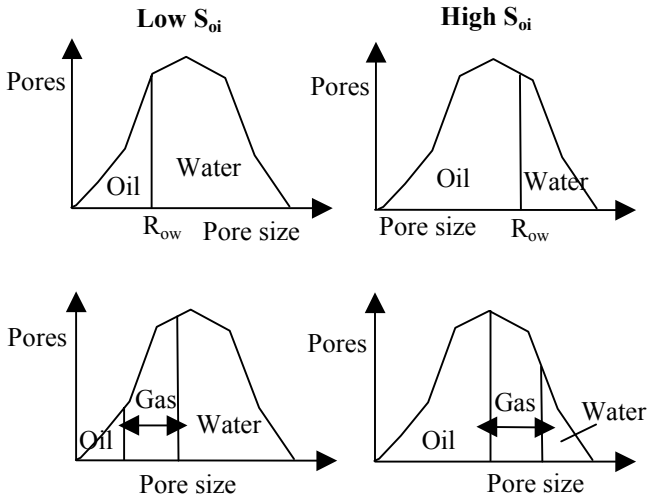

Fig. 10. Schematic pore occupancies for an oil-wet system. For two-phase flow, oil resides in the small pores and water in the large pores. Gas is intermediate-wet and displaces both oil and water, starting by displacing pores with radii close to R_{ow}, the radius of the largest water-filled pore after water injection. For large S_{oi} and R_{ow}, gas occupies larger pores than for small S_{oi}, resulting in a larger gas relative permeability.

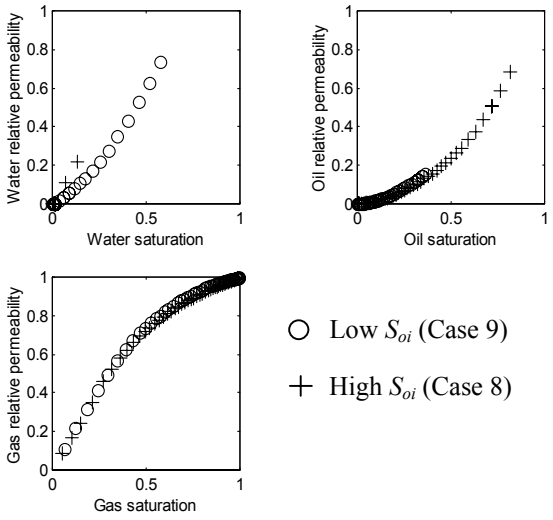

Fig. 11. Three-phase relative permeabilities for a weakly oil-wet system. Water is the intermediate-wet phase. The gas and oil relative permeabilities do not depend on S_{oi}, while the water relative permeability does.

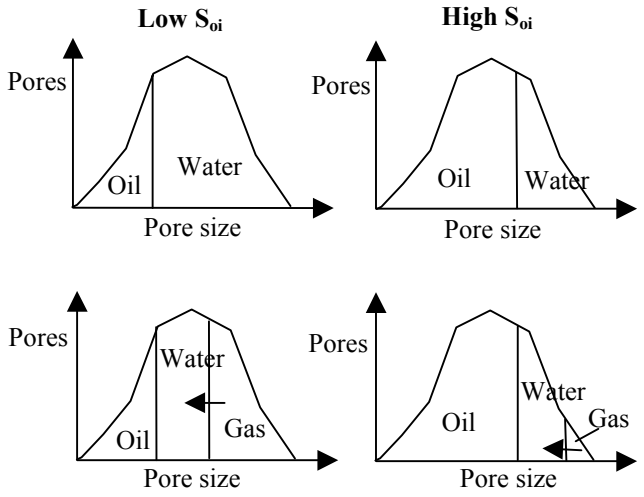

Fig. 12. Schematic pore occupancies for a weakly oil-wet system. For two-phase flow, oil resides in the small pores and water in the large pores. Gas is non-wetting to oil and water. Gas invades the largest water-filled pores first. Water is intermediate-wet. For large S_{oi} water occupies larger pores than for small S_{oi}, at the same water saturation, resulting in a larger water relative permeability.

Fractionally-Wet Media. Many porous media are fractionally-wet, meaning that different regions of the pore space have different wettabilitities. We could model this by allowing different pores to have different contact angles. For simplicity, we did not consider these cases. However, it is possible that with combinations of pores that fall into all three of the generic wettability types, the relative permeabilites of all three phases could be functions of two independent saturations. Empirical models of three-phase relative permeability need to be able to allow all three relative permeabilities to depend on two saturations.[44,51]

A full analysis of the different possible functionalities for capillary pressure and relative permeability for a bundle of circular cylindrical capillary tubes has recently been presented by van Dijke et al.[52] Fractionally-wet media were considered explicitly and the ranges of saturation for which the relative permeabilities depended on one or more saturations were found.

Conclusions

We have found ten fluid configurations in a single pore for three-phase flow in mixed-wet systems. The displacement sequence was primary drainage with wettability alteration, followed by waterflooding and gas injection. We found the capillary pressures for all possible displacements and analyzed oil and water layer formation and stability. We gave approximate expressions for the fluid conductances. This analysis is a first step in the development of a predictive pore-scale model of three-phase flow in mixed-wet media.

To illustrate the effects of wettability in three-phase flow we computed relative permeabilites for a bundle of capillary tubes. The results for water-wet media – a quadratic oil layer drainage regime and the effect of spreading coefficient – agree with previous theoretical and experimental work.[10,39,40]

Oil forms wetting layers in gas-occupied pores that persist down to low oil saturation with a characteristic layer drainage regime for the oil relative permeability. The only exceptions are non-spreading oils in water-wet media, or large gas/oil contact angles.

The relative permeability of the phase of intermediate wettability depends on both its own saturation and S_{oi}, while the other relative permeabilities are functions of their own saturation only. In water-wet media, oil is the intermediate-wet phase. In weakly oil-wet media, water is intermediate-wet. In most strongly oil-wet media, gas is intermediate-wet. For media that contain regions of different wettabilitites, all three relative permeabilities may depend on both their own saturation and S_{oi}.

Nomenclature

A = area, L^2, m^2.
b = length of water-wet corner, L, m.
C = dimensionless curvature.
C_{so} = oil spreading coefficient, F/L, N/m.
f = boundary condition label.
g = conductance, L^4, m^4.
k_r = relative permeability.
L = length, L, m.
n_c = number of corners for a pore.
P = pressure, F/L^2, Pa.
P_c = capillary pressure, F/L^2, Pa.
Q = volumetric flow rate, L^3/T, m^3/s.
r = radius of curvature, L, m.
R = inscribed pore radius, L, m.
S = saturation.
S_g = gas saturation.
S_o = oil saturation.
S_{oi} = initial oil saturation before gas injection.
S_w = water saturation.
α = half-angle of a corner of a pore.
β = angle.
γ = exponent.
δ = exponent.
ϕ = conductance parameter.
μ = viscosity, M/L/T, $kgm^{-1}s^{-1}$.
θ = contact angle.
θ_0 = contact angle during primary drainage before wettability change.
θ_1 = contact angle during primary drainage after wettability change.
θ_{ow} = oil/water contact angle during water injection.
θ_{go} = gas/oil contact angle during gas injection.
θ_{gw} = gas/water contact angle during gas injection.
σ = interfacial tension, F/L, N/m.
Ω = effective perimeter, L, m.

Subscripts

c = corner.
$crit$ = critical.
eff = effective.
g = gas.
h = hinging.
max = maximum.
min = minimum.
o = oil.
s = solid or surface.
t = total.
w = water.

Superscripts

max = maximum.

Acknowledgments

The authors are grateful to Pål-Eric Øren, Ken Sorbie and Rink van Dijke for many helpful suggestions and comments. The members of the Stanford University Gas Injection Affiliates Group (SUPRI-C) and the Heriot-Watt/Stanford/Imperial consortium on pore-scale modeling (BP Amoco, Arco, Statoil, Elf, Enterprise Oil, Exxon, Shell, JNOC, and the Department of Trade and Industry) are thanked for their financial support.

References

1. Jerauld, G. R.: "General Three-Phase Relative Permeability Model for Prudhoe Bay," SPE 36178 proceedings of the 7th ADIPEC, Abu Dubai, 13-16 October 1996.
2. Jerauld, G. R.: "Prudhoe Bay Gas/Oil Relative Permeability," *SPE Reservoir Engineering*, **12**:66-73, 1997.
3. Øren, P.-E., Billiote, J., and Pinczewski, W. V.: "Mobilization of Waterflood Residual Oil by Gas Injection for Water-Wet Conditions," *SPE Formation Evaluation*, **7**:70-78, March 1992.
4. Øren, P.-E., and Pinczewski, W. V.: "Fluid Distribution and Pore Scale Displacement Mechanisms in Drainage Dominated Three-phase Flow," *Transport in Porous Media*, **20**:105-133, 1995.
5. Soll, W. E., Celia, M. A., and Wilson, J. L., "Micromodel Studies of Three-Fluid Porous Media Systems: Pore-Scale processes Relating to Capillary Pressure - Saturation Relationships," *Water Resources Research*, **29**(9):2963-2974, 1993.
6. Kantzas, A., Chatzis, I., and Dullien, F. A. L.: "Enhanced Oil Recovery by Inert Gas Injection," SPE 13264 proceedings of the Sixth SPE/DOE Symposium on Enhanced Oil Recovery, Tulsa, OK, April 1988.
7. Dong, M., Dullien, F. A. L., and Chatzis, I.: "Imbibition of Oil in Film Form Over Water Present in Edges of Capillaries with an Angular Cross-section," *J. Colloid & Interface Science*, **172**:278-288, December 1995.
8. Keller, A. A., Blunt, M. J., and Roberts, P. V.: "Micromodel Observation of the Role of Oil Layers in Three-phase Flow," *Transport in Porous Media*, **20**:105-133, 1997.
9. Heiba, A. A., Davis, H. T., and Scriven, L. E.: "Statistical Network Theory of Three-Phase Relative Permeabilities," SPE 12690 proceedings of the SPE/DOE Symposium on Enhanced Oil Recovery, Tulsa, OK, April 15-18, 1984.
10. Fenwick, D. H., and Blunt, M. J.: "Network Modeling of Three-Phase Flow in Porous Media," *SPE Journal*, **3**:86-97, 1998a.
11. Fenwick, D. H., and Blunt, M. J.: "Three-Dimensional Modeling of Three-phase Imbibition and Drainage," *Advances in Water Resources*, **25**(2):121-143, 1998b.
12. Mani, V., and Mohanty, K. K.: "Pore-Level Network Modeling of Three-Phase Capillary Pressure and Relative Permeability Curves," *SPE Journal*, **3**:238-248, September 1998.
13. Øren, P.-E., Billiote, J., and Pinczewski, W. V.: "Pore-Scale Network Modelling of Waterflood Residual Oil Recovery by Immiscible Gas Flooding," SPE/DOE 27814, proceedings of the Ninth SPE/DOE Symposium on Improved Oil Recovery, Tulsa, OK, April 1994.
14. Morrow, N. R., Lim, H. T., and Ward, J. S.: "Effect of Crude-Oil-Induced Wettability Changes on Oil Recovery," *SPE Formation Evaluation*, **1**(February):89-103, 1986.
15. Fassi-Fihri, O., Robin, M., and Rosenberg, E.: "Wettability Studies at the Pore Level: Anew Approach by the Use of Cryo-Scanning Electron Microscopy," SPE 22596, proceedings of the SPE Annual Conference, Dallas, 1991.
16. Mohanty, K. K., and Salter, S. J.: "Multiphase Flow in Porous Media: Part 3 – Oil Mobilization, Transverse Dispersion and Wettability," SPE 12127, proceedings of the SPE Annual Conference, San Francisco, 1983.
17. Heiba, A. A., Davis, H. T., and Scriven, L. E.: "Effect of Wettability on Two-Phase Relative Permeabilities and Capillary Pressures," SPE 12172, proceedings of the SPE Annual Conference, San Francisco, 1983.
18. McDougall, S. R., and Sorbie, K. S.: "The Impact of Wettability on Waterflooding: Pore-Scale Simulation," *SPE Reservoir Engineering*, **10**(August): 208-213, 1995.
19. Dixit, A. B., McDougall, S. R., Sorbie, K. S., and Buckley, J. S.: "Pore-Scale Modeling of Wettability Effects and Their Influence on Oil Recovery," *SPE Reservoir Evaluation and Engineering*, **2**(February): 25-36, 1999.
20. Kovscek, A. R., Wong, H., and Radke, C. J.: "A Pore-Level Scenario for the Development of Mixed Wettability in Oil Reservoirs," *AIChE Journal*, **39**(6):1072-1085, 1993.
21. Blunt, M. J.: "Pore Level Modeling of the Effects of Wettability," *SPE Journal*, **2**(December):494-510, 1997.
22. Blunt, M. J.: "Physically-Based Network Modeling of Multiphase Flow in Intermediate-Wet Porous Media," *Journal of Petroleum Science and Engineering*, **20**:117-125, 1998.
23. Øren, P.-E., Bakke, S., and Arntzen, O.J.: "Extending Predictive Capabilities to Network Models," *SPE Journal*, **3**:324-336, December 1998.
24. Man, H. N., and Jing, X.-D.: "Network Modelling of Wettability and Pore Geometry Effects on Electrical Resistivity and Capillary Pressure," *Journal of Petroleum Science and Engineering*, **24** (in press) 2000.
25. Ma, S., Mason, G., and Morrow, N. R.: "Effect of Contact Angle on Drainage and Imbibition in Regular Polygonal Tubes," *Colloids and Surfaces A: Physiochemical and Engineering Aspects*, **117**:273-291, 1996.
26. Buckley, J. S., and Liu, Y.: "Some mechanisms of crude oil/brine/solid interactions," *Journal of Petroleum Science and Engineering,* **20**:155-160, 1998.
27. Mayer, R. P., and Stowe, R. A.: "Mercury Porosimetry-Breakthrough Pressure for Penetration between Packed Spheres," *Journal of Colloid and Interface Science*, **20**:893-911, 1993.

28. Princen, H. M.: "Capillary Phenomena in Assemblies of Parallel Cylinders I. Capillary Rise between Two Cylinders," *Journal of Colloid and Interface Science*, **30**:60-68, 1969.
29. Princen, H. M.: "Capillary Phenomena in Assemblies of Parallel Cylinders II. Capillary Rise with More Than Two Cylinders," *Journal of Colloid and Interface Science*, **30**:359-365, 1969.
30. Princen, H. M.: "Capillary Phenomena in Assemblies of Parallel Cylinders III. Liquid Columns between Horizontal Parallel Cylinders," *Journal of Colloid and Interface Science*, **34**:171-180, 1970.
31. Bryant, S., and Blunt, M. J.: "Prediction of Relative Permeability in Simple Porous Media," *Physical Review* A, **46**:2004-2011, August 1992.
32. Zhou, D., Blunt, M., and Orr, F. M. Jr.: "Hydrocarbon Drainage along Corners of Noncircular Capillaries," *Journal of Colloid and Interface Science*, **187**:11-21, 1997.
33. Firincioglu, T., Blunt, M. J., and Zhou, D.: "Three-Phase Flow and Wettability Effects in Triangular Capillaries," *Colloids and Surfaces A*, **155**:259-276, 1999.
34. Ransohoff, T. C., and Radke, C. J.: "Laminar Flow of a Wetting Fluid along the Corners of a Predominantly Gas-Occupied Noncircular Pore," *Journal of Colloid and Interface Science*, **121**:392-401, 1988.
35. Zhou, D. and Blunt, M. J., "Effect of Spreading Coefficient on the Distribution of Light Non-Aqueous Phase Liquid in the Subsurface," *Journal of Contaminant Hydrology*, **25**:1-19, 1997.
36. Kalaydjian, F. J.-M., Moulu, J.-C., and Vizika, O.: "Three-phase Flow in Water-Wet Porous Media: Determination of Gas/Oil Relative Permeabilities Under Various Spreading Conditions," SPE 26671 proceedings of the SPE Annual Conference, Houston, October 3-6, 1993.
37. Adamson, A. W.: *Physical Chemistry of Surfaces*, fifth edition, John Wiley & Sons, New York City, 1990.
38. Vizika, O. and Lombard, J.-M.: "Wettability and Spreading: Two Key Parameters in Oil Recovery With Three-Phase Gravity Drainage," *SPE Reservoir Engineering*, **11**:54-60, 1996.
39. Sahni, A., Burger, J. E., and Blunt, M. J.: "Measurement of Three-phase Relative Permeability during Gravity Drainage Using CT Scanning," SPE 39655 proceedings of the SPE/DOE 11th Symposium on Improved Oil Recovery, Tulsa, OK, April 1998.
40. DiCarlo, D. A., Sahni, A., and Blunt, M. J.: "Effect of Wettability on Three-phase Relative Permeability," SPE 40567 proceedings of the SPE Annual Conference, New Orleans, September 1998.
41. Blunt, M. J., Zhou, D., and Fenwick, D. H.: "Three-phase Flow and Gravity Drainage in Porous Media," *Transport in Porous Media*, **20**:77-103, 1995.
42. Stone, H. L.: "Probability Model for Estimating Three-Phase Relative Permeability," *Journal of Petroleum Technology*, 214-218, February 1970.
43. Baker, L. E.: "Three-Phase Relative Permeability Correlations," SPE 17369 proceedings of the SPE/DOE Symposium on Enhanced Oil Recovery, Tulsa, OK April 17-20, 1988.
44. Blunt, M. J.: "An Empirical Model for Three-Phase Relative Permeability," SPE 56474 proceedings of the SPE Annual Conference, Houston, 1999.
45. Oak, M. J., Baker, L. E., and Thomas, D. C.: "Three-phase Relative Permeability of Berea Sandstone," *Journal of Petroleum Technology*, **42**:1057-1061, August 1990.
46. Oak, M. J.: "Three-Phase Relative Permeability of Water-Wet Berea Sandstone," SPE 20183 proceedings of the SPE/DOE Seventh Symposium on Enhanced Oil Recovery, Tulsa OK, April 22-25, 1990.
47. Baker, L. E.: "Three-Phase Relative Permeability of Water-Wet, Intermediate-Wet and Oil-Wet Sandstone," proceedings of the Seventh European Symposium on Improved Oil Recovery, Moscow, October 1993.
48. Skauge, A., Eleri, O. O., Graue, A. And Monstad, P., "Influence of Connate Water on Oil Recovery by Gravity Drainage," SPE 27817 proceedings of the SPE/DOE Ninth Symposium on Improved Oil Recovery, Tulsa, OK April 17-20, 1994.
49. Eleri, O. O., Graue, A., and Skauge, A.: "Steady-State and Unsteady-State Two-Phase Relative Permeability Hysteresis and Measurements of Three-phase Relative Permeabilities Using Imaging Techniques," SPE 30764 proceedings of the SPE Annual Conference, Dallas, 22-25 October, 1995.
50. Nordtvedt, J. E., Ebeltoft, E., Iversen, J. E., Sylte, A, Urkedal, H., and Vatne, R. F.: "Determination of Three-Phase Relative Permeabilities From Displacement Experiments," SPE 36683 proceedings of the SPE Annual Conference, Denver, October 6-9, 1996.
51. Hustad, O. S. and Hansen, A. G.: "A Consistent Correlation for Three-phase Relative Permeabilities and Phase Pressures Based on Three Sets of Two-phase Data," proceedings of the Eighth European Symposium on Improved Oil Recovery, Vienna, May 15-17 (1995).
52. van Dijke, R., McDougall, S., and Sorbie, K. S.: "A Process-Based Approach for Three-Phase Capillary Pressure and Relative Permeability Relationships in Mixed-Wet Systems," SPE 59310, proceedings of the SPE/DOE Symposium on Improved Oil Recovery, Tulsa, April 2000.